sustainability

IMPACT FACTOR 3.3

CITESCORE 6.8

Article

Enhancing Efficiency of Grid-Connected Solar Photovoltaic System with Particle Swarm Optimization & Long Short-Term Memory Hybrid Technique

Ramakanta Jena, Ritesh Dash, Kalvakurthi Jyotheeswara Reddy, Prasanta Kumar Parida, Chittathuru Dhanamjayulu, Sarat Chandra Swain and S. M. Muyeen

MDPI

https://doi.org/10.3390/su15118535

sustainability

MDPI

Article

Enhancing Efficiency of Grid-Connected Solar Photovoltaic System with Particle Swarm Optimization & Long Short-Term Memory Hybrid Technique

Ramakanta Jena [1], Ritesh Dash [2], Kalvakurthi Jyotheeswara Reddy [2], Prasanta Kumar Parida [3], Chittathuru Dhanamjayulu [4,*], Sarat Chandra Swain [5] and S. M. Muyeen [6,7,*]

[1] Department of Electrical Engineering, Seemanta Engineering College, Mayurbhanj 757086, India; rjenafel@gmail.com
[2] School of Electrical and Electronics Engineering, REVA University, Bengaluru 560064, India; rdasheee@gmail.com (R.D.)
[3] School Of Rural Management, KIIT Deemed to be University, Patia, Bhubaneswar 751024, India; prasanta.parida@ksrm.ac.in
[4] School of Electrical Engineering, Vellore Institute of Technology, Vellore 632014, India
[5] School of Electrical Engineering, KIIT Deemed to be University, Patia, Bhubaneswar 751024, India; scs_132@rediffmail.com
[6] Department of Electrical Engineering, Qatar University, Doha 2713, Qatar
[7] School of Electrical Engineering, Computing and Mathematical Sciences, Curtin University, Perth 6102, WA, Australia
* Correspondence: dhanamjayulu.c@vit.ac.in (C.D.); sm.muyeen@qu.edu.qa (S.M.M.)

Abstract: Maximum Power Point Tracking (MPPT) is a technique used in photovoltaic (PV) systems to maximize the power output from the solar panel by constantly tracking and adjusting the optimal operating point. To achieve this, various algorithms have been developed, with Particle Swarm Optimization (PSO) being a widely used method. By adjusting the control system's parameters, PSO can determine the optimal operating point of the solar panel and improve its overall performance. PSO employs swarm intelligence by simulating the behavior of particles to find the best solution for a given problem. Long Short-Term Memory (LSTM) belongs to the family of Recurrent Neural Networks (RNN) in machine learning and is designed to address the limitations of traditional RNNs in capturing long-term dependencies that exist in sequential data. The combination of PSO and LSTM techniques can result in an efficient MPPT algorithm that leverages the benefits of both. PSO is utilized to optimize the control parameters of the MPPT algorithm, while LSTM is used to predict the solar panel's power output based on historical data. Consequently, this integration can lead to an accurate and efficient MPPT algorithm that can effectively track the solar panel's maximum power point. In this research article, an effort has been made to control the duty cycle of the converter by suitably controlling the system gain. A Matlab-based Simulink model in conjunction with Python programming has been used to make the system more robust.

Keywords: algorithm; GA; PSO; PSO-LSTM; search space

Citation: Jena, R.; Dash, R.; Reddy, K.J.; Parida, P.K.; Dhanamjayulu, C.; Swain, S.C.; Muyeen, S.M. Enhancing Efficiency of Grid-Connected Solar Photovoltaic System with Particle Swarm Optimization & Long Short-Term Memory Hybrid Technique. *Sustainability* **2023**, *15*, 8535. https://doi.org/10.3390/su15118535

Academic Editor: Luis Hernández-Callejo

Received: 8 March 2023
Revised: 8 May 2023
Accepted: 9 May 2023
Published: 24 May 2023

1. Introduction

Electricity consumption is increasing at a faster rate than any other form of energy worldwide, creating a perpetual challenge due to socioeconomic growth. The use of fossil fuels is declining, yet the rate of consumption to support the industrial revolution is still high. Traditional sources are insufficient to meet the ever-growing energy demands, causing concerns about energy security and rising fossil fuel prices. The urgent need to find compatible options has led to increased research and development in renewable energy sources such as solar and wind power, which are widely accessible [1,2]. Solar energy is particularly promising due to its abundance and potential to meet global energy needs.

Photovoltaic cells (Solar PV) are a leading option for energy technology due to their direct conversion of solar radiation into electrical energy [3]. However, there are still significant challenges to overcome, such as fluctuating energy, low energy conversion efficiency, and high energy costs. To address these challenges, researchers are working to enhance the power output of photovoltaic modules through Maximum Power Point Tracking (MPPT), which matches the characteristics of the module to deliver maximum power output and prevent power loss.

The foremost objective of the MPPT technique is to reduce oscillations due to changing weather conditions and to achieve fast and accurate tracking performance by controlling the operating point of the converter to operate the system constantly at Maximum Power Point (MPP) for regularisation of the output of the PV device [4,5]. The principal goal of the MPPT is to extract the highest power from the PV device. By locating the MPP and adjusting the duty ratio of the converter, the MPPT technique reduces the power loss and improves the conversion efficiency [6–8].

Various MPPT methods such as Perturb and Observation (P&O), Incremental Conductance (IC), fractional short circuit current, fractional open-circuit voltage, and advanced techniques based on Neural Network (NN), Fuzzy Logic (FL), bio-inspired optimization, and nature-inspired optimization are discussed in [9,10]. It has been observed that the most popular P&O MPPT algorithm has some benefits of smooth implementation, simple structure, and low cost. The PV output power is altered with small constant steps in each cycle. The regulating parameters are PV current and voltage, which is known as the perturbation. The *P&O* method fails under rapidly changing environmental conditions due to its high convergence speed [11,12]. The traditional algorithms prove to be efficient in steady irradiance conditions. Up to 70% power, loss occurs with sudden alteration in irradiance, and they fail to track the global peak. The traditional techniques exhibit a lot of global peaks and local peaks, and they fail to locate the global peaks [13].

The global peaks are tracked properly by bio-inspired optimization methods such as ant colony optimization, artificial bee colony, flower pollination, cuckoo search, and Particle Swarm Optimization (PSO) [14]. Under a steady state, the above optimization techniques exhibit oscillations. Salp-Swarm Optimization Algorithm (SSA) [15], Whale Optimization Algorithm (WOA) [16], Grey Wolf Optimization (GWO) [17], and Harris hawk optimization [18] are some other meta-heuristic techniques. The GWO is better in terms of speed and accuracy, and the WOA technique tracks the GP with higher accuracy and speed. To improve the convergence rate of the *P&O* technique, it can be combined with an Artificial Neural Network (ANN) [19], which is known for its faster convergence rate. The *P&O* tracks the peak operating point, and then the ANN locates the Peak (GP). To improve the convergence rate and to reduce the steady-state oscillation, *P&O* is combined with the WOA technique in [20]. The *P&O* algorithm is used to locate the optimum operating point, while the WOA algorithm is used to find the GP at the initial stage with a higher rate of convergence.

The non-linear complex problems are easily solved by machine learning approaches. Extreme machine learning technology is used for the prediction of solar power by solving the short-term nonparametric probabilistic theory. The solution to forecasting issues related to solar power is presented in [21], using an LSTM. In this article, the authors proposed an enhanced PSO method by integrating LSTM and optimizing the LSTM parameters. This approach updates the speed equation and improves particle attraction in the PSO structure, thereby enhancing the selection of initial parameters of the LSTM structure to forecast the output power of the PV system.

The article [22] presents a new hybrid approach that combines PSO and LSTM to improve the performance of MPPT in PV systems when dealing with partially shaded conditions. The method employs PSO to optimize MPPT control parameters and LSTM to predict the solar panel's power output based on historical data. The study compares the proposed approach with conventional MPPT algorithms under various partially shaded

conditions, and the results show that the hybrid PSO-LSTM approach achieves higher accuracy and efficiency.

The non-linear complex problems are easily solved by machine learning approaches. Extreme machine learning technology is used for the prediction of solar power by solving the short-term nonparametric probabilistic theory. The forecasting issues of solar power are solved by an LSTM. The accuracy of the power fluctuation forecasting is improved by estimating the solar panel tilt angle. An improved particle swarm optimization is proposed in this article by combining long short-term memory and particle swarm optimization by optimizing the parameters of LSTM. The speed equation is updated, and the particles are attracted in the PSO structure, which improves the selection of initial parameters of the LSTM structure to forecast the output power of the PV system.

A novel MPPT approach for PV systems under partial shading conditions has been proposed [23]. The proposed method uses a combination of PSO and LSTM neural networks to improve the accuracy and efficiency of the MPPT process. The PSO algorithm is used to optimize the parameters of the LSTM network, which is trained to predict the MPP under different shading conditions accurately. The proposed PSO-LSTM method is compared with other MPPT techniques, and simulation results show that the proposed method outperforms the other methods in terms of accuracy, speed, and efficiency. The proposed PSO-LSTM method can be an effective solution for improving the performance of PV systems under partial shading conditions.

The paper [24] proposes the hybrid marine predator sine cosine algorithm (HMPSCA) to optimize the parameters of a hybrid active power filter (HAPF) that mitigates harmonic distortions caused by nonlinear loads. The algorithm combines the marine predator and sine cosine algorithms to improve the convergence speed and accuracy. The performance of the HMPSCA is compared with other optimization algorithms, such as PSO and genetic algorithm (GA), based on the convergence rate and objective function value. The results indicate that the HMPSCA outperforms other algorithms and achieves better suppression of harmonic distortion.

Based on the literature survey on the present state of art model, the following key contribution has been proposed in the present research article.

- Mathematical modeling of the PSO-LSTM MPPT model has been carried out in this research article.
- The validation of the proposed PSO-LSTM MPPT with other established models under partial shading conditions has been performed as an integral part of this paper.
- Hardware implementation of the model has been carried out for robustness evaluation of the model under different weather conditions.

The remaining paper is organized as follows: in Section 2, the problem formulation is discussed. Section 3 depicts the benchmarking model. Section 4 presents numerical simulations to verify the effectiveness of our approach and conclusions are given in Section 5.

2. Problem Formulation

Figure 1 shows the variation of MPP under different solar irradiance over a time domain $t \; \forall \; t \;\; \in \;\; T$. A subject graph of Figure 1 is shown in Figure 2, representing maximum power deviation ΔP and right load side to MPP here referred to as oscillating area. The inhomogeneous waveform of Figure 2 can be analyzed using Neumann and Dirichlet boundary control methods. Therefore, let us consider a Distributed Control Boundary (DCB) for the variable solar power around MPP. Here curve-1 and curve-3 can be considered as a DCB for curve-2. Therefore,

$$DCB = \begin{cases} \min_{p,v\in(P,V)} M(p,v) := \frac{1}{2}||\Delta P||^2_{RT} + \frac{\alpha}{2}||\Delta V||^2_{RT} \\ \min_{i,v\in(I,V)} M(i,v) := \frac{\sqrt{3}}{2}|\frac{\Delta P}{||\Delta V||}|_{RT} \\ \underset{-\Delta P=0}{ST} \;\; \forall \;\; \Delta Pm \;\in\; |R| \;\; and \\ v \;\in\; V_{MPP} \;\subset\; V_{OC} \end{cases} \tag{1}$$

Here, Equation (1) is a derived equation by applying the gradient stochastic probability to the increasing slope of the incremental conductance-based MPPT curve. $M_{(p,v)}$ represents the maximum power point (MPP) on the PV curve. To minimize the oscillations around the MPP, it has been designed as a minimization type of function. $M(i,v)$ represents the projected maximum power point from the PV curve to the IV curve. $|R|$ represents the universe of discourse containing all the data points of the PV plane, the condition is valid subject to (ST) change in maximum power with respect to reference observation as a negative change in slope. V_{MPP} shows the maximum power with reference to voltage and V_{OC} represents the open circuit voltage of SPV module.

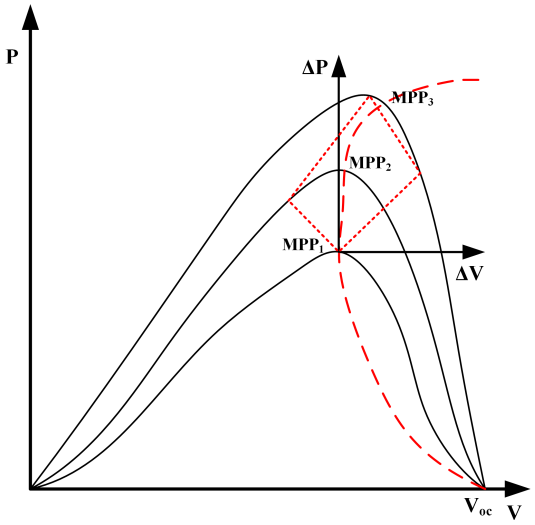

Figure 1. PV curve of a typical MPPT system.

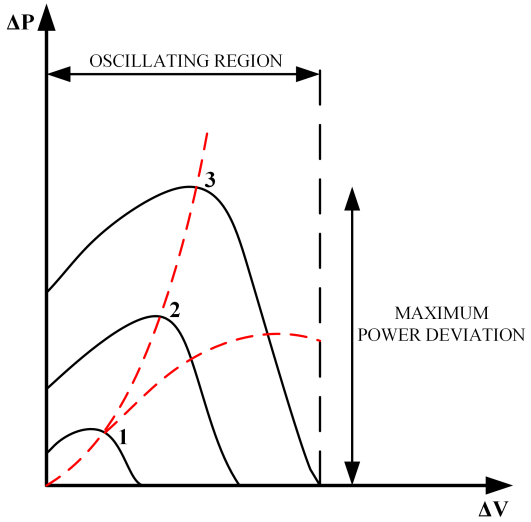

Figure 2. Rate of change in PV curve of a typical MPPT system showing oscillation region.

The solution for Equation (1) can be analyzed by equating $M : V \rightarrow R^2(\rho)$ with $\rho = \partial R$, where ∂ represents the partial differential equation with respect to $\partial p, \partial v$ i.e., $\frac{\partial R}{\partial p \partial v}$. Therefore, it is understood that there exists a weak sense between MPP and its boundary [25,26]. This can be analyzed by considering N-R-type boundary control and Robin-type boundary control.

2.1. N-R Type Boundary Control

The equivalent DCB of Equation (1) can be written as

$$DCB = \begin{cases} \min_{p,v\in(P,V)} M(p,v) := \frac{1}{2}||\Delta P||^2_{RT} + \frac{\alpha}{2}||\Delta V||^2_{RT} \\ \underset{-\Delta P=0}{ST} \quad \forall\ \Delta Pm\ \in\ |R| \\ \partial_n P = f(BV - \Upsilon p) \\ v\ \in\ V_R \leq V_{oc} \end{cases} \tag{2}$$

Here in Equation (2), B represents the Boltzmann constant for oscillating voltage V, and that of Y_p represents the present state of voltage. $\partial_n P$, represents the 'n' number of oscillating observed maximum power. Equation (2) equivalently can be written as

$$\min_{u\in V_R} \hat{M}(v) \tag{3}$$

Again the function $\hat{M}(v) := M(p(v), v) \equiv M(SBV, v)$ over surface V_R, where $S : p^* \rightarrow p\ for\ p := H^{'}(\Omega)$ becomes a weak solution operator. Here, p^* represents the new updated power (p). Therefore, the stiffness function value becomes

$$D(p,v) = \int_R \nabla p\ \nabla v\ dP\ + \int_T \Upsilon p v_R d\rho = f(v)|_{p^* p},\ (V_R) \in P \tag{4}$$

In Equation (4), $f(v)|_{p^* p}$ represents the instantaneous voltage magnitude as a function of present and immediate past power magnitude on the PV curve. Whereas $(V_R) \in P$ represents any value of V inside the region of convergence which belongs to P on the PV plane. Again as an action of BV on the performance of Equation (4) as an element $R(BV)\ \in\ p^*$ can be defined as

$$\int_R f(BV), V\rangle|_{p^*,p} = \int_R BV v\ dR\ , \forall\ V_{oc} \in V \tag{5}$$

The contour integral of $\int_R f(BV), V\rangle|_{p^*,p}$, results in the partial integral of BV over the contour R, where every single solution can be modeled as a function of V. Therefore, Equation (5) can be redesigned as a convergent function of a unique solution, satisfying first-order boundary conditions such that

$$\langle M(v), V - v\rangle|_{p^*,p} \geq\ \forall\ v \in V_R \tag{6}$$

Equation (6) represents that the optimization problem can be made dependent on controller parameters for the active dynamic conditions of operation [27,28]. It is completely characterized by Maximum Power Point curve-1 (MPP_1) and Maximum Power Point curve-3 (MPP_3).

The function $M(v)$ in Equation (6) can be integrated with Poisson's equation and Neumann boundary condition as

$$\begin{cases} -\Delta M(v) = p - \Delta P_o|_{R\in(P,V)} \\ \partial_R p + vp = 0\ R \cap (P,V) \end{cases} \tag{7}$$

On applying Equation (7) to Equation (6) with variational inequality, Equation (6) can be reduced to

$$\langle \hat{M}_p(V_p), v - V_p\rangle V_R^*\ \geq 0\ \forall\ v \in V_R \tag{8}$$

or

$$\hat{M}_p(P) = \alpha V + B^* P_p(v) \tag{9}$$

In Equation (8), V_R^* represents the updated resultant voltage on the PV curve, and in Equation (9), B^* represents the updated Boltazman's multiplication factor after the second derivative.

2.2. Robin Type Boundary Value

The equivalent optimization Equation (3) can be modified as

$$minM(p,v) = \frac{1}{2}\int_{R_{MPP1}} (V(T(G_0 - p))^2)d(T) + \frac{\alpha}{2}\int_{R_{MPP2}} V(T,G_0)^2 d\sigma(T,G_0) + \int_{R_{MPP3}} V(T,G_0)d\sigma(T,G_0) \quad (10)$$

$$S.T = \begin{cases} (p,v) \in H_R^{'} X R^2(T,G_0) \\ V \in V_R = v \in R^2(\rho) \; \forall 0 \leq v(T,G_0) \leq 1 \end{cases} \quad (11)$$

In Equation (10), R_{MPP1}, R_{MPP2}, and R_{MPP3} represents the resistances associated with different curves [29,30] Similarly, $H_R^{'}$ represents state space matrix of contour R and G_0 represents reference irradiance.

Figure 3 Represents the surface view for Equations (7) and (10) with different boundary value conditions. The Robin boundary condition defines the correlation between the values of a function and its normal derivative at the boundary of a domain and is a common type of boundary condition in partial differential equations. This establishes a relation between local minima and the slope of the MPPT curve, which is an integral objective of this research.

The PI-controlled MPPT has been used along with the SPV grid-connected system for easy control of the system. However, the tuning of gain parameters such as proportional gain (K_p) and integral gain (K_i) uses the PSO-LSTM methodology. This enables the dynamic update of K_p and K_i value with respect to changes in loading pattern at PCC. The LSTM will create a range of values for both the gain so that during transient disturbances such as partial shading and loading switching, the gain can slide over the derived range.

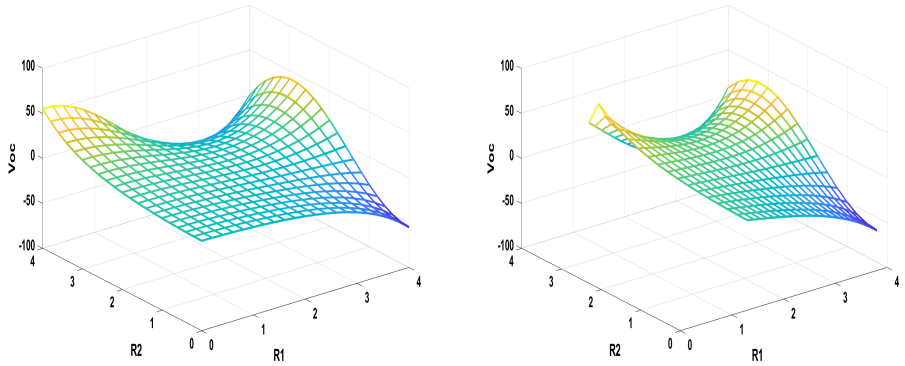

(**a**) (**b**)

Figure 3. *Cont.*

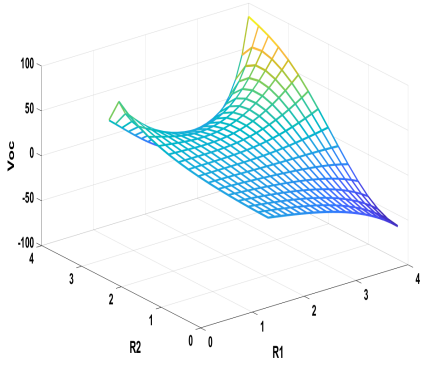

(**c**)

Figure 3. (**a**) General surface view of Equation (1), (**b**) surface view of Equation (7) with N-R type boundary control, and (**c**) surface view of Equation (10) with Robin type boundary control.

3. Bench Marking Model

To check the efficiency and robustness of the proposed model, two benchmarking models have been considered for comparison. The benchmarking models are Genetic Algorithm MPPT (GA-MPPT) and PSO-MPPT.

3.1. Case-1: GA-MPPT

The principle of natural evolution can be embodied with maximum power point tracking in terms of genetic algorithm. The selection, mutation, and cross-over concept of the genetic algorithm in terms of fitness value can be applied to different power levels in an MPPT. Each individual inside the MPPT will be assigned as an agent and fitness value as a stochastic function of their characteristics [31,32]. The detailed structure of an individual with chromosome level is shown in Figure 4.

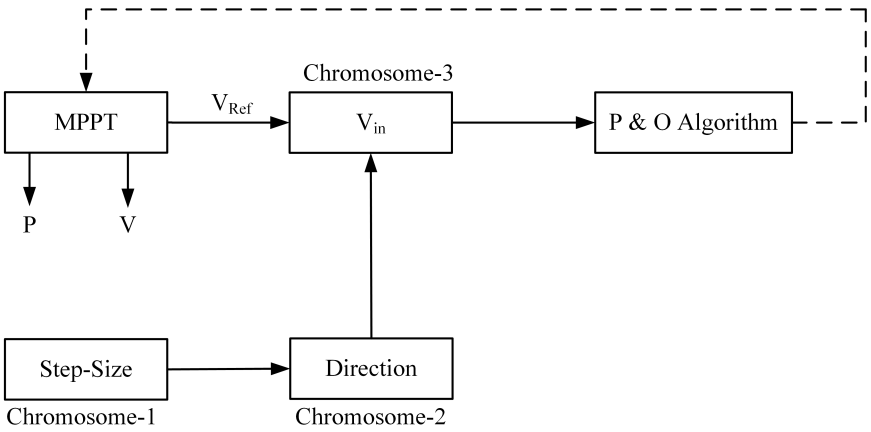

Figure 4. Chromosome model for MPPT analysis.

Here it can be observed that Chromosome-3 (Figure 4) sets the operating voltage for MPPT. The reference value will be set up as a function of power and voltage at MPP. The next two chromosomes will decide the step size and direction of the MPPT optimization direction and steepness value.

As a function of the genetic algorithm, the operating points will be generated based on the parent selection characterized by individual steepness value. On the PV curve, two pints will be randomly chosen to produce a set of offspring based on the parameters as shown in Table 1.

During the process of optimization like cross-over and selection, if GMPP is found same from parent to child, then it is assumed that this is the MPP, and the corresponding value of P and V_{oc} will be taken into consideration for the generation of the necessary duty cycle.

Figure 5 shows the cross-over operation of the identified right-hand side point of oscillation in the parent PV curve. The operation will identify either a positive slope or a negative slope along with the direction of movement of the MPP. Therefore, the output of the GA-MPPT can be modeled as a function of both voltage and step size [33,34].

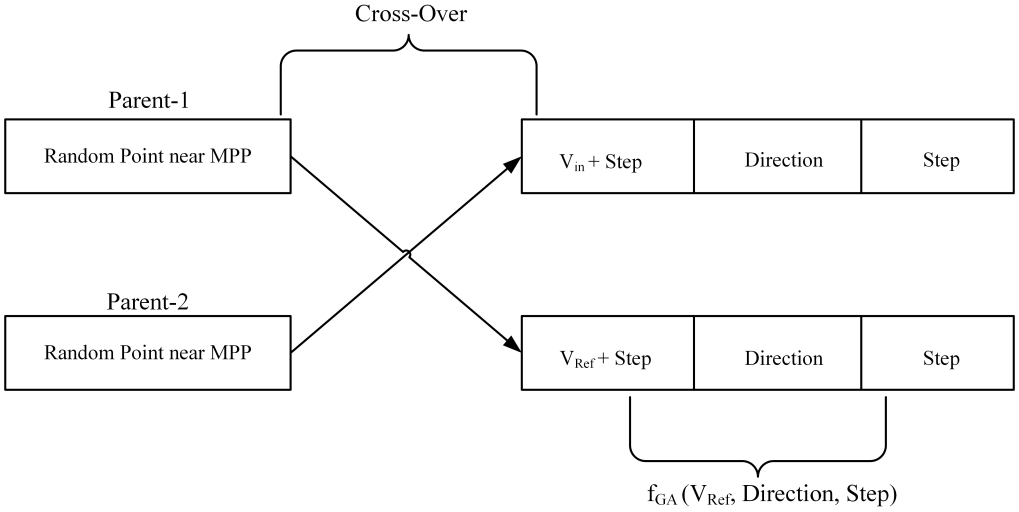

Figure 5. Crossover operation of parent curve in MPPT.

Figure 6a shows the probability oscillation movement of P and V_{oc} with a variance of 0.77. Here the system predicts three different oscillation points near the MPP (Algorithm 1, Pseudo-code) with an estimated direction of movement. Again, from the estimated direction, it can also be found that the system is more dominant towards the right-hand side against the left-hand side on the PV curve [35]. Similarly, Figure 7 shows the GA performance for a variance of 0.92.

Algorithm 1: Evaluating MPP for perturb$\leq$ 0.2 s. using GA

1. Initialize probability vector
2. Select two parents in the PV curve
$P_i \rightarrow P_1$
$P_{i+\delta t} \rightarrow P_2$
3. $Evaluate(P_1) and (P_2)$
4. While GA has not converged()
$P_{12}(t) \leftarrow P(t)$ Parent selected
$P_c(t) \leftarrow P_{12}(t)$ Reproduction
Mutation $P_c(t)$
Evaluate $P_e(t)$
$P(t+1) \leftarrow$ Build, Evaluate next-generation data
Change $t \leftarrow t+1$
end while
5. Return the best result for evaluation

Table 1. Parameters for genetic algorithm selection, mutation, crossover.

	n = 10	**n = 20**	**n = 30**
Population Size	100	200	300
Probability of Cross over	0.7	0.71	0.75
Elite Size	1%	1%	1%
% of mutation	10%	10%	10%
Stopping Criteria	error = 0.1	error = 0.1	error = 0.1
Cross Over	Uniformly Mapped	Uniformly Mapped	Uniformly Mapped
Cross Over Type	CC = 0.1	CC = 1	CC = 1
Selection Criteria	Stochastic Movement	Stochastic Movement	Brownian Movement
Fitness	90%	90%	100%

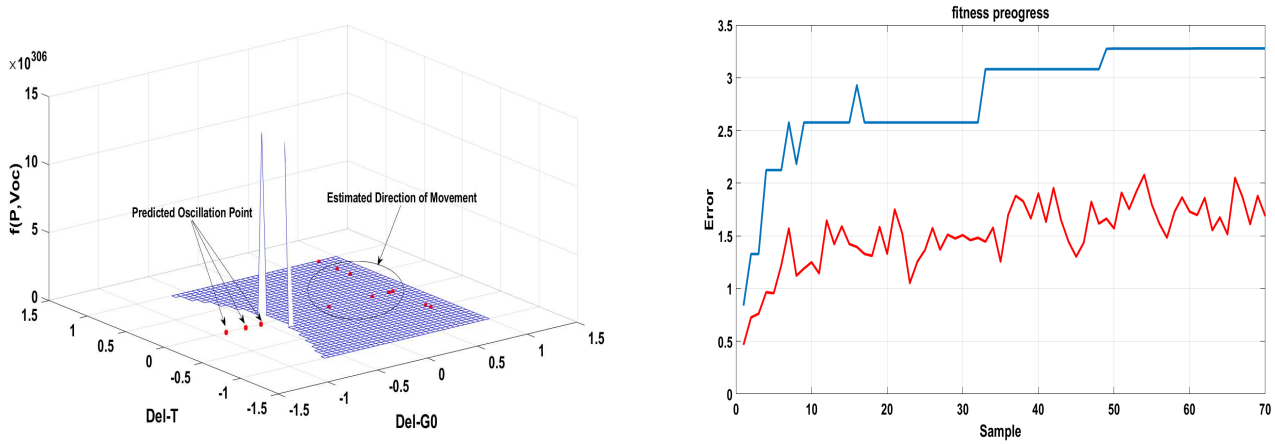

(**a**) (**b**)

Figure 6. Probability oscillation movement: (**a**) change in P and V_{oc} as a function gene movement with variance = 0.77; (**b**) fitness progress response.

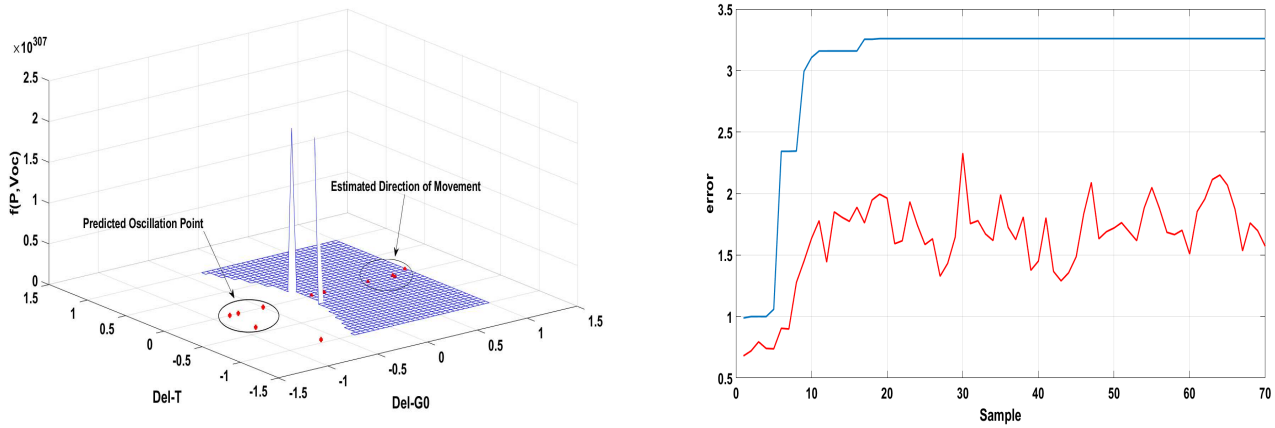

(**a**) (**b**)

Figure 7. Probability oscillation movement: (**a**) change in P and V_{oc} as a function gene movement with variance = 0.92; (**b**) fitness progress response.

3.2. Case-2: PSO-MPPT

One of the universally used bio-inspired models in optimization theory is PSO. The output of the solar voltaic system greatly depends upon solar irradiance and environmental temperature leading to a nonlinear output characteristic in terms of convergence and constraint optimization. This makes the system have more than one number of local minima and global minima. Some of the optimization algorithms get locked in the local minima leading to a non-convergence solution [35,36].

In multi-dimensional cooperative optimization, the genetic algorithm does not make the system converge; therefore, PSO has been chosen as an optimization algorithm. To apply PSO in the present content of MPPT, let us assume that each particle is at the initial position P_i with an initial velocity of P_i in the defined search space. Each individual particle inside the search space is characterized by P_{best} and as a whole G_{best}. Combining both the velocity along with their characteristic, the swarm velocity can be written as

$$V_i^{k+1} = \omega V_i^k + c_1 r_1 (P_{best} - P_i^k) + c_2 r_2 (G_{best} - P_i^k) \tag{12}$$

$$P_i^{k+1} = P_i^k + V_i^{k+1} \tag{13}$$

Here the velocity of the swarm has been controlled by two random variables called r_1 and r_2, respectively. Therefore, the convergence time is highly dominated by the proper selection of this variable at the initial point of time. The random variable of a larger size may omit the convergence point. Therefore, the step difference between the two conjugate points should not be more than 1×10^{-3}.

Again, in the same equation, k represents the number of iterations required for convergence, and ω represents the initial selected weight for each particle. In the present research context of right-hand side MPPT optimization, the search space is limited to $\frac{\delta p}{\delta \omega}$ greater than zero. The required amount of duty cycle has been made as a function of particle velocity. This shows that if $r = 1$, then the unity power factor can be achieved at the terminal of the solar inverter. The slow moment of the particle leads to a sluggish response with a less-duty cycle.

Again, from the P_i controlled MPPT techniques, it is noticed that the K_i and K_p value lies in the range of [0.47–0.62] and [0.33–0.41], respectively. Therefore, in the present research, an initial search space has been probed with an upper boundary of K_i and K_p, respectively. In comparison to the P_i controller, where the tuning of K_p and K_i is based on the Nichols–Ziegler method, which can be made dynamic by using the PSO-based tuning. This ultimately decreases the net searchable area in the MPPT and, thus, reduces the local oscillations around the MPP. Therefore, Equations (7) and (10) can be modified into the following two equations:

$$V_i^{k+1} = \omega V_i^k + c_1 \rho_1 (P_{best} - P_i^k) + c_2 \rho_2 (G_{best} - P_i^k) \tag{14}$$

and

$$P_i^{k+1} = P_i^k + V_i^{k+1} \tag{15}$$

The performance of the particle sum optimization can be enhanced by making the system more populated. Here, four cluster analyses for three identified points on the MPPT curve have been conducted. Each cluster in the net consists of 72 numbers of swarms. The detailed response is shown in Figure 8.

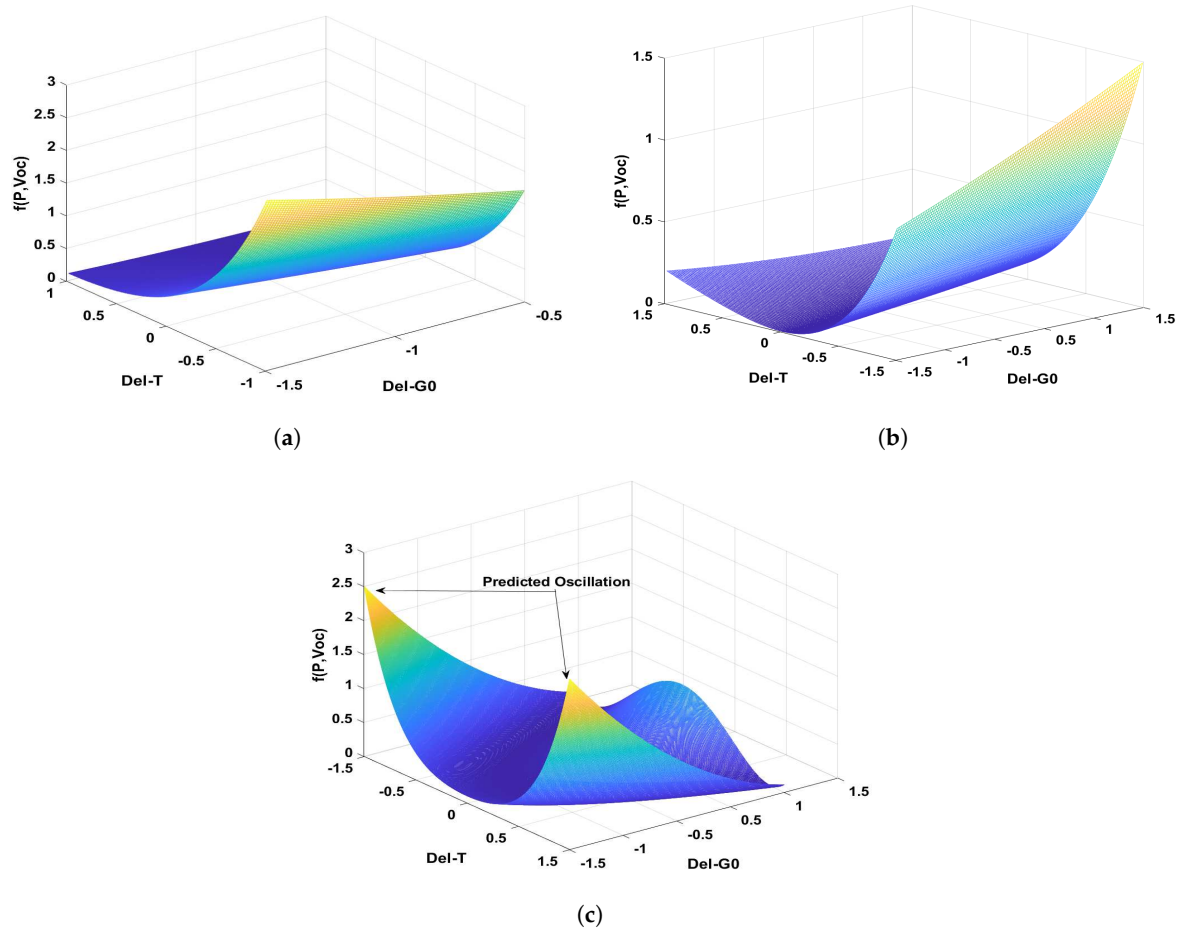

Figure 8. Change in P and V_{oc} as a function of particle movement inside PSO. (**a**) Initial Position (P_i) = 0.1 and Initial velocity (V_i) = 1.03; (**b**) Initial Position (P_i) = 0.3 and Initial velocity (V_i) = 1.03; (**c**) Initial Position (P_i) = 0.5 and Initial velocity (V_i) = 1.03.

4. Simulation and Result Analysis

To validate the proposed algorithm, a hardware setup (Figures 9 and 10) with programmable D-space has been implemented with a solar panel for its effective analysis and a detailed comparative study with other commercially available MPPT algorithms. As observed in Figure 10, all the experimental setup has been established at Standard temperature conditions (STC) only. Two types of experimental testbeds have been created, such as for dusty surface evaluation of SPV and partial shading conditions. The PSO-LSTM flowchart for the process is presented in Figure 11. The detailed technical specification of the hardware setup system is shown in Table 2.

In this research work, the effectiveness of the proposed algorithms has been evaluated with three different case studies, such as partial shading, dusty surface, and greenhouse gas concentration.

Again, before starting the analysis, it is required to choose the proper activation function for the LSTM MPPT model. Table 3 shows the analysis of the LSTM algorithm with four different types of activation functions under normal operating conditions. As observed, ReLu took 12.03 ms. time to reach 80% of the final time for MPP, whereas Softmax is taking the highest time of 12.97 ms to achieve the same position. Again ReLU is showing a voltage level of 38.91 V for $0.9V_{oc}$ against $0.7V_{oc}$ of 31.14. Hence, for analysis of LSTM with the MPPT algorithm, in this paper ReLu activation function has been used.

Table 2. Detailed technical specifications of SPV model.

Sr. No,	Parameter	Rating
1	Wattage rating of solar Panel	400 wp
2	Open circuit voltage at STC	43.2 V
3	MPP voltage at STC	38.7 V
4	Short circuit current of panel	6.79 A
5	MPP current at STC	6.51 A
6	No. of series connected panels	7
7	No. of parallel connected panels	66
8	DC-DC converter output voltage	407 V
9	Boost converter rating	4 KW
10	Inductor rating	6 mH
11	Filter inductance	252 NH
12	Inverter type	3 level, VSI

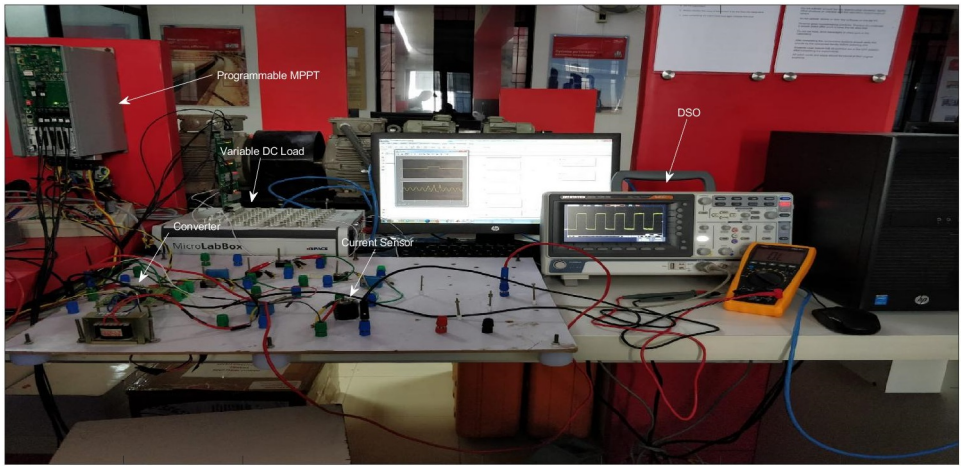

Figure 9. MPPT Experimental Setup for Partial Shading.

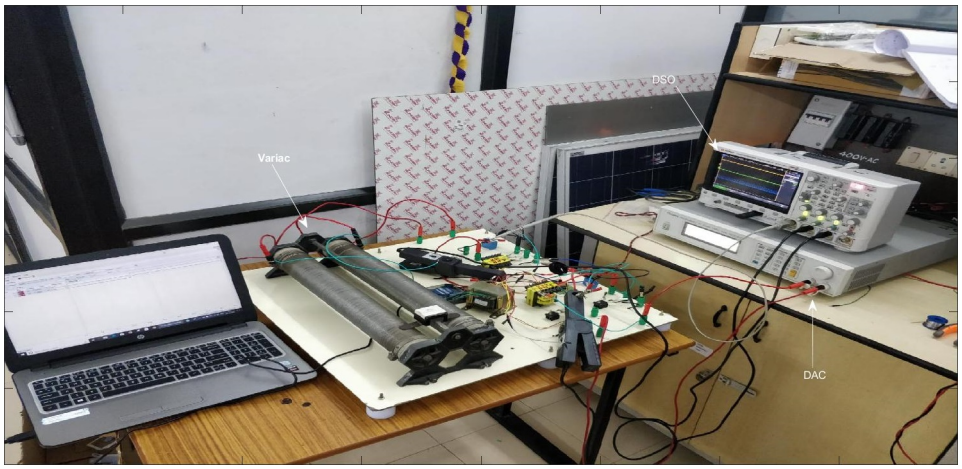

Figure 10. MPPT Experimental Setup for Color Spectrum.

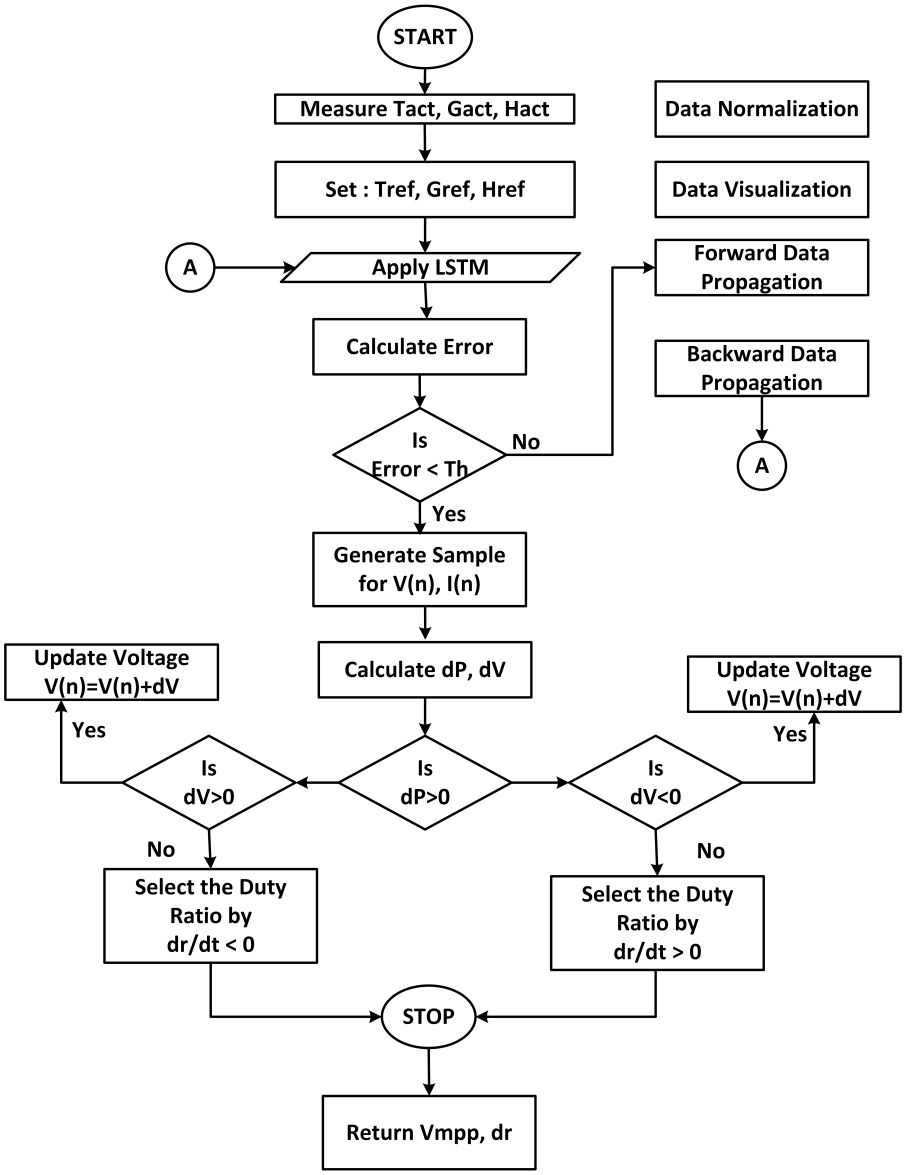

Figure 11. PSO-LSTM process flow chart for generation of duty cycle under different testing condition.

Table 3. Performance of Different activation functions under varying SPV parameter

% **Type of Activation**	V_{oc}			**Time**	
	0.9V_{oc}	**0.8V_{oc}**	**0.7V_{oc}**	**0.9 T**	**0.8 T**
sigmoid	38.88	34.56	30.24	13.76	12.04
tanh	38.10	33.17	29.63	13.23	12.00
ReLu	38.91	34.59	31.14	13.16	12.03
Softmax	38.63	33.70	30.16	13.55	12.97

Figure 12 shows the block diagram of LSTM-enabled P&O MPPT for duty cycle generation. Hereafter, data normalization, both forward and backward sweep, has been applied for proper training of the data set, which ultimately leads to better forecasting and selection of activation function. Again, in this architecture, 100 hidden networks have been taken into consideration for reducing the R^2 error. Finally, the duty cycle will be evaluated through a Fuzzy logic evaluator. The LSTM enabled MPPT will create a reference MPP for

P&O and thereby minimizing the search space.

Case-1: Partial Shading Condition

Shading is an unavoidable effect in solar PV systems. The *P&O* algorithm oscillates around the maximum power point under varying partial shading conditions. To analyze the effectiveness of the proposed PSO-LSTM MPPT algorithm, a 50% shading effect in three clusters has been applied over the solar PV panel.

Basically, LSTM is affected by the type of activation function used in the system. Therefore, a comparative analysis of different types of activation functions with LSTM has been investigated.

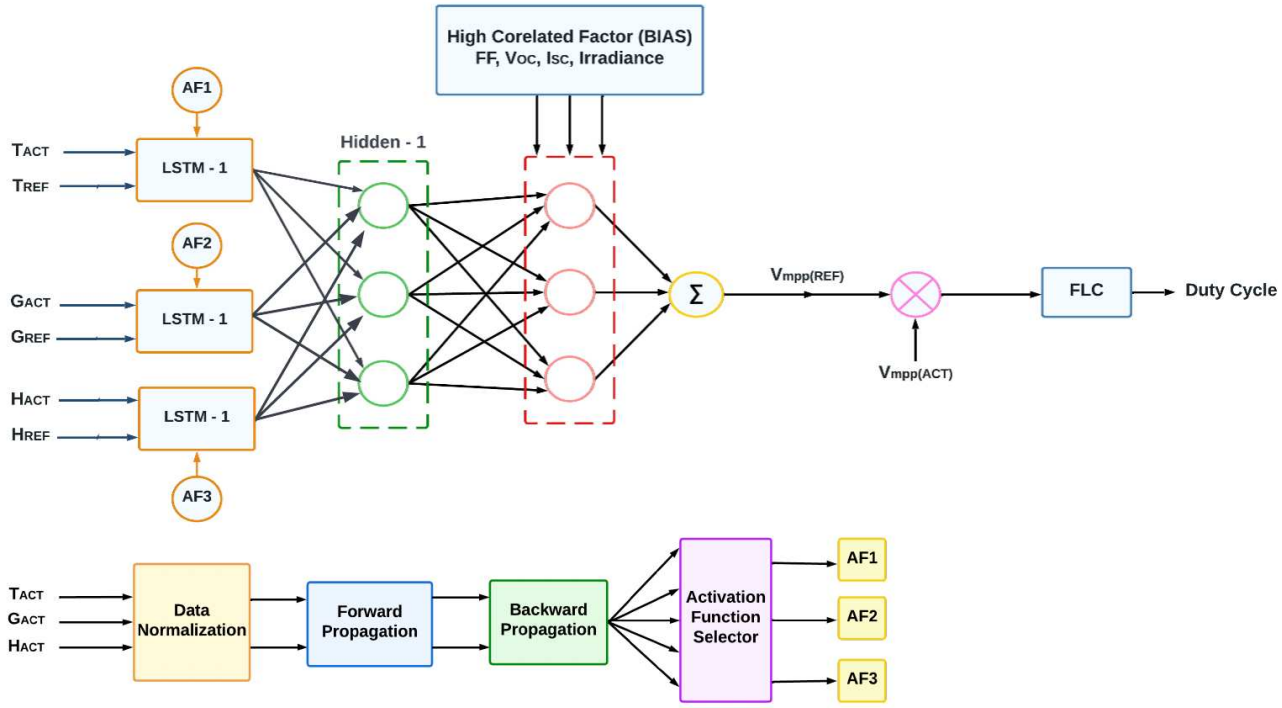

Figure 12. Block diagram of LSTM enabled P and O MPPT for duty cycle generation.

Table 4 shows the cluster analysis of partial shading with PSO-LSTM. Relu activation function has been used in LSTM to evaluate the performance. As mentioned, five different clusters with transient disturbance of 10% to 50% have been used. It is observed that the tracking time increased to 39.63 ms for 50% transient partial shading against 11.93 ms for 10% transient shading. Gain a minimum MPP has been observed to be 153.0 W_p and that of maximum 376.8 W_p occurs at 10% transient partial shading.

Table 4. MPP max and min data.

Cluster	% Shading (Transient)	MPP max	MPP min	Standard Deviation	Tracking Time (s)
C-1	10	376.8	359.1	13.09	11.93
C-2	20	364.5	357.8	11.83	11.27
C-3	30	322.4	304.6	18.06	13.06
C-4	40	298.6	272.9	24.33	17.18
C-5	50	173.1	153.0	34.49	39.63

Table 5 shows the comparative analysis of different MPPT algorithms under normal and partial shading conditions. Here the analysis has been carried out for the percentage of oscillations along with tracking efficiency. It is found that for PSO-LSTM MPPT, the efficiency is 93.47%, with the percentage of oscillations around 2.83 for normal conditions.

Similarly, with under-average partial shading of 25%, the tracking efficiency for PSO-LSTM MPPT is found to be 83.27% with the percentage of oscillations around 9.26, which is 89.48% better as compared to GA MPPT and 87.23% efficient as compared to PSO MPPT under same conditions.

Table 5. A comparative analysis of different MPPT algorithms under normal and partial shading condition.

Condition	Type of MPPT Algorithm	MPP Tracking Time	% of Oscillations	Tracking Efficiency
Normal	GA	8.33	4.11	85.88
	PSO	6.98	3.82	89.31
	PSO-LSTM	6.36	2.83	93.47
Partial Shading	GA	17.04	9.43	78.66
	PSO	15.81	9.68	81.05
	PSO-LSTM	9.83	9.26	83.27

Figure 13 shows the characteristic evaluation for LSTM output and target along with the error curve under partial shading conditions. It is observed that the system has shown a maximum oscillation of 42% of shading condition, where LSTM efficiently distinguishes the MPP from the local convergence areas. At the same time, maintaining an accuracy level of 87.4%.

Figure 14 represents the histogram plot with 20 Bins for Instances against error under partial shading conditions. As observed, for an error of +1.42, the system shows 13.44 instances with a validation level of 27%. Similarly, Figure 15 shows the LSTM performance for Correlation and Lag under partial shading conditions. The system has an autocorrelation level of 0.027.

Case-2: Dusty Surface

Most of the time, solar panels are installed outside the building, in open space, or on the top of the roof. Therefore, it is obvious that it is highly affected by the dust. The MPPT controller must be designed in such a manner that it should be least affected by dust and other disturbances. In this research work, three different types of dust, such as L, M, and H-class, have been applied on the surface of a solar panel for the effectiveness of the MPPT performance. The three types of dust have been applied over three clusters. Table 6 shows the performance of solar PV under different dusty conditions with the proposed algorithm.

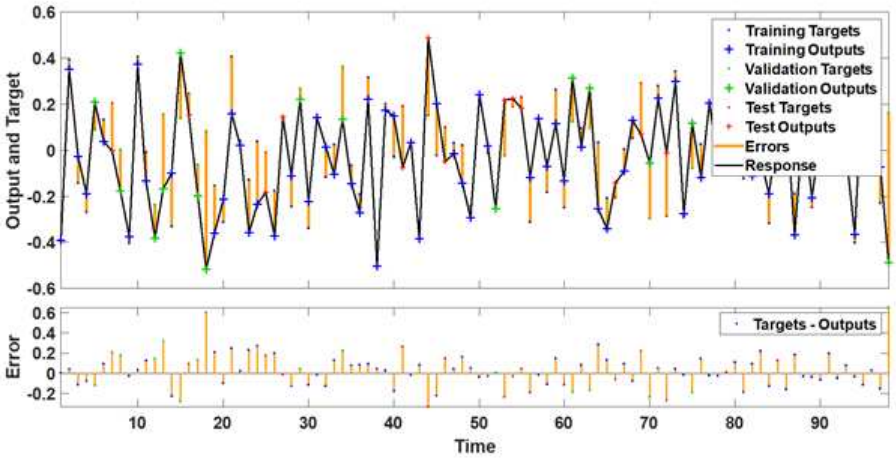

Figure 13. Characteristic evaluation for LSTM output and target along with the Error curve under partial shading condition.

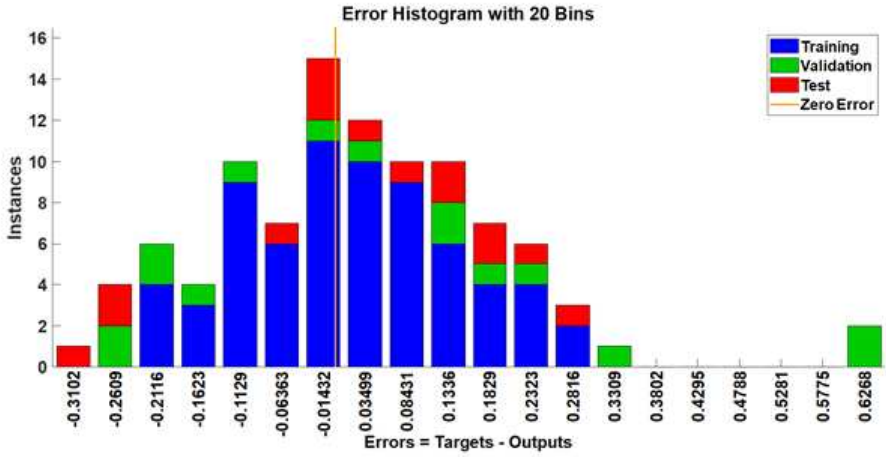

Figure 14. Histogram plot with 20 Bins for Instances against error under partial shading condition.

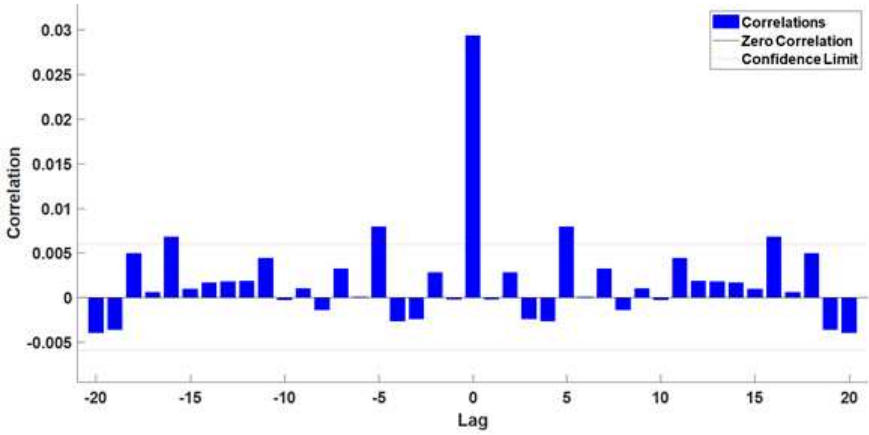

Figure 15. LSTM performance for Correlation and Lag under partial shading condition.

Table 6. Performance of solar PV under different dusty conditions with proposed algorithm.

Type of Dust	% of Mixture	MPP max	MPP min	SD	Tracking Time (ms)
L-Type	10%	382.66	381.07	9.63	5.41
	20%	373.04	372.91	9.65	5.07
	30%	366.19	358.82	8.87	4.93
M-Type	10%	379.93	375.04	11.44	8.10
	20%	353.27	349.84	11.16	8.33
	30%	344.64	341.73	12.29	8.67
H-Type	10%	352.97	339.18	23.01	12.31
	20%	347.11	328.09	18.84	17.44
	30%	323.74	304.68	18.35	24.89

Table 7 shows the cluster analysis of dusty surfaces, where a comparative analysis of the proposed system has been carried out under different percentages of concentration of dust. It is observed that for 30% of L-type dust, the tracking time is 4.93, whereas, for H-type of dust, it is 24.89. Similarly, a standard deviation of 18.35 has been observed for 30% concentration of H-type dust, and that of 12.29 has been observed for M-type dust levels. Therefore, on average, it can be concluded that the proposed system is robust in terms of tracking and speed of operation observed in Table 7.

Table 7. Comparative analysis of the algorithm under different percentages of concentration of dust.

Type of Algorithm	% of Dust	MPP Tracking Time	% of Oscillations	Tracking Efficiency
GA	10	17.36	7.84	89.93
	20	19.98	10.07	86.22
	30	23.43	11.63	77.48
PSO	10	17.27	8.03	90.96
	20	19.66	10.39	88.30
	30	23.19	10.58	81.54
PSO-LSTM	10	17.16	7.42	91.36
	20	18.59	9.86	89.91
	30	21.64	10.18	83.43

Figure 16 shows the characteristic evaluation for LSTM output and target along with the error curve under dusty surface conditions. It is observed that the system has shown a maximum oscillation of 26%, where LSTM efficiently distinguishes the MPP from the local convergence areas. At the same time, maintaining an accuracy level of 89.01%.

Figure 17 represents the histogram plot with 20 Bins for Instances against error under dusty surface conditions. As observed, for an error of +0.048, the system shows 10.31 instances. Similarly, Figure 18 shows the LSTM performance for Correlation and Lag under dusty surface conditions. The system has an autocorrelation level of 0.015.

Case-3: Green House Gas Concentration

Although greenhouse gas concentration does not have a direct impact on the performance of solar PV panels, they create a large amount of heat as a function of albedo, which ultimately increases the surface temperature of SPV. This extra increase in temperature has an adverse effect on the performance of SPV. Hence in the present research, it has been included for effective evaluation of the proposed controller.

Table 8 shows the performance of PSO-LSTM MPPT under different concentrations of GHGs. It is observed that for CO_x with 1.7 kg of GHG, the tracking time is 7.22 ms, and that of for NO_x and CO_x at the same concentration, it is 6.69 ms and 6.83 ms, respectively. Again, a minimum MPP of 355.66 and a maximum MPP of 383.48 has been observed for CO_x and NO_x, respectively.

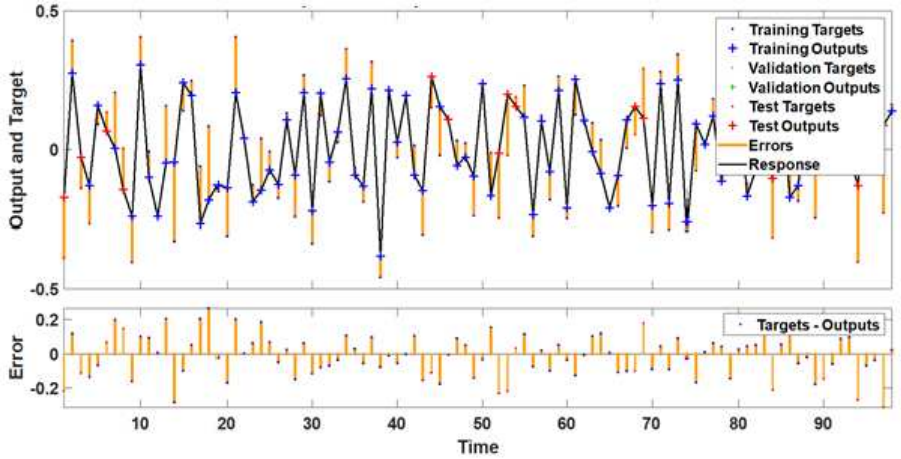

Figure 16. Characteristic evaluation for LSTM output and target along with the Error curve under dusty surface conditions.

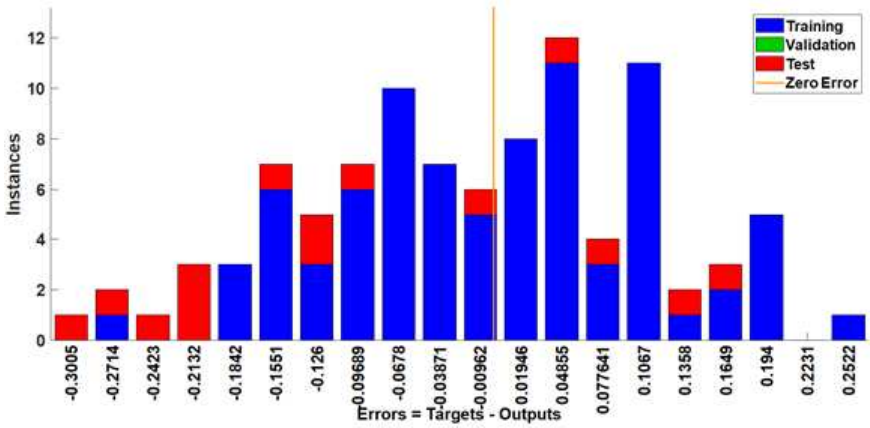

Figure 17. Histogram plot with 20 Bins for Instances against error under dusty surface conditions.

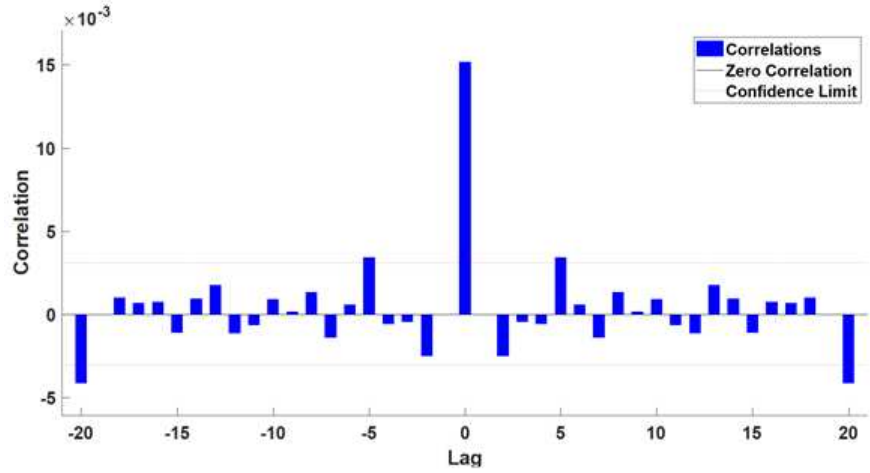

Figure 18. LSTM performance for Correlation and Lag under dusty surface conditions.

Table 8. Performance of PSO-LSTM MPPT under different concentrations of GHGs.

Type of GHG	Weight of GHG	MPP max	MPP min	Standard Deviation	Tracking Time
CO_X	0.8 kg	381.02	379.64	9.84	6.34
	1.3 kg	378.33	371.83	9.62	6.78
	1.7 kg	361.78	355.68	9.63	7.22
NO_X	0.8 kg	381.66	381.08	2.44	6.84
	1.3 kg	381.39	381.00	1.85	6.81
	1.7 kg	377.19	376.94	3.82	6.69
SO_X	0.8 kg	383.48	381.13	1.04	6.91
	1.3 kg	379.26	379.22	1.16	6.90
	1.7 kg	381.35	380.88	2.37	6.83

Figure 19 shows the Characteristic evaluation for LSTM output and target along with the error curve under the greenhouse gas concentration (CO_x) condition. It is observed that the system has shown a maximum oscillation of 39%, where LSTM efficiently distinguishes the MPP from the local convergence areas. At the same time, the PV system maintains an accuracy level of 93.19%.

Figure 20 represents the Histogram plot with 20 Bins for Instances against error under the greenhouse gas (CO_x) condition. As observed, for an error of –0.052, the system shows 8.33 instances. Similarly, Figure 21 shows the LSTM performance for Correlation and Lag under the greenhouse gas (CO_x) condition. The system has an autocorrelation level of 0.026.

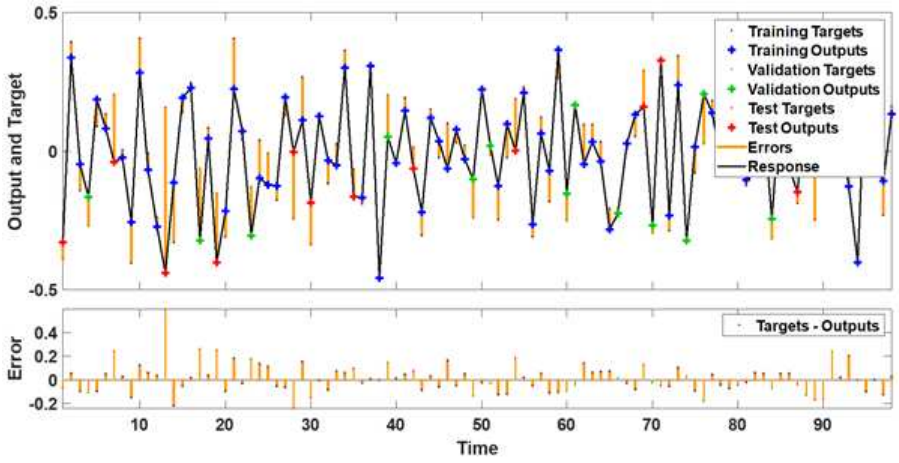

Figure 19. Characteristic evaluation for LSTM output and target along with Error curve under greenhouse gas concentration (CO_x) condition.

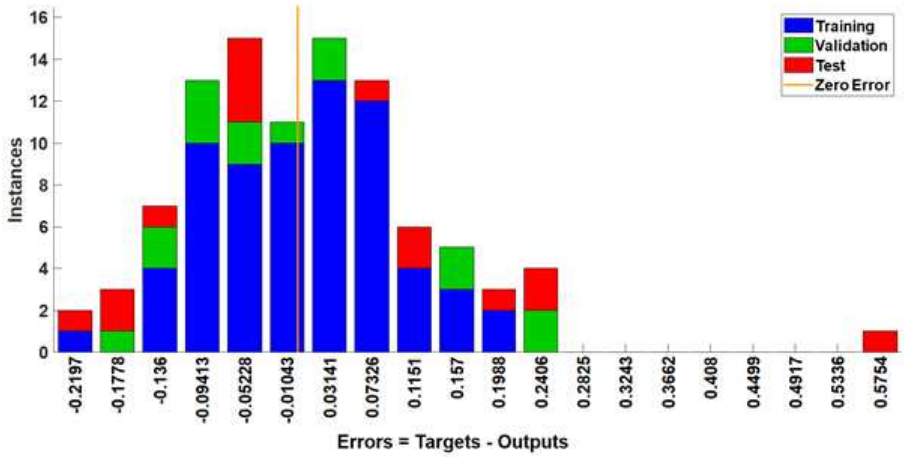

Figure 20. Histogram plot with 20 Bins for Instances against error under greenhouse gas (CO_x) condition.

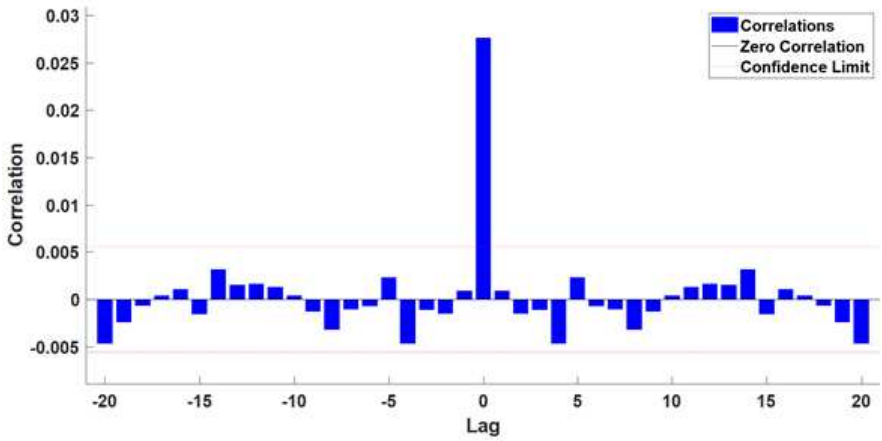

Figure 21. LSTM performance for Correlation and Lag under greenhouse gas (CO_x) condition.

Figure 22a shows the reference voltage in the blue color line and that of actual voltage in the red color line for MPPT-Boost Converter and Figure 22b represents modulation index, with PSO-LSTM under partial shading condition. The PI controller in a DC-DC converter constantly compares the reference voltage and the actual DC link voltage to produce a control signal. This control signal is used to modify the converter's switching

behavior in order to regulate the output voltage. By monitoring the discrepancy between the reference and actual voltages, the PI controller adjusts the converter's duty cycle or switching frequency to minimize the error and maintain the actual DC link voltage in proximity to the desired reference voltage. This closed-loop control mechanism allows the converter to accommodate variations in load, input voltage, and external conditions, thereby ensuring stable and precise voltage regulation. As observed, the system maintains a constant voltage at the output of the converter from 1.5 s onwards. However, a little perturb has been observed at 0.5 s and 1.33 s due to the change in the action of MPP. In other words, it can also be described as the searching time instances for the PSO-LSTM algorithm. Again, from Tables 6 to 8, it is also understood that the system is taking only 17 ms. to track the new MPPT point against traditional MPP control action. Similarly, the modulation indexed has been maintained at 1 unit throughout the work.

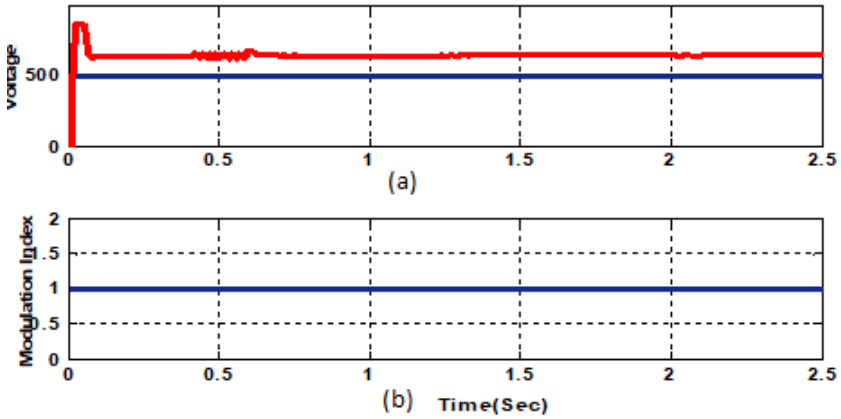

Figure 22. Performance of Vref–Vmean & Modulation Index with PSO-LSTM under partial shading condition.

Figure 23a reference voltage in violet color line and that of actual voltage in red color line for MPPT-Boost Converter and Figure 23b represents modulation Index, with PSO-LSTM under dusty surface condition. During transient conditions, it is essential for the actual DC link voltage, which indicates the measured output voltage of the converter, to closely track the reference voltage. This tracking is achieved through the comparison of the actual voltage with the reference voltage by the controller, which then generates a control signal to appropriately adjust the converter's operation. To effectively compensate for disturbances and variations in load, the controller must exhibit a rapid and robust response. This ensures that the converter swiftly adapts to transient changes, minimizing deviations between the actual and desired voltages and maintaining a stable and reliable output. Here the system maintains a steady output voltage of 420 V. However, during the H-type dust conditions, the system is exhibiting maximum oscillations. The system takes 43.71 ms to relocate to a new MPP.

Figure 24 shows the Performance of the Vref–Vmean modulation index with PSO-LSTM under greenhouse gas conditions. Figure 24a represents Vref and Vmean in time, while Figure 24b stands for percentage modulation in time. As observed system exhibits small oscillations during the initial interval of time. This is because of the increase in temperature due to the greenhouse gas effect. As a consequence, overall, it can be said that direct greenhouse has no effect on the performance of the PV; however, indirectly, it traps the temperature, which ultimately increases the surface temperature of the system and thereby affects the system behavior.

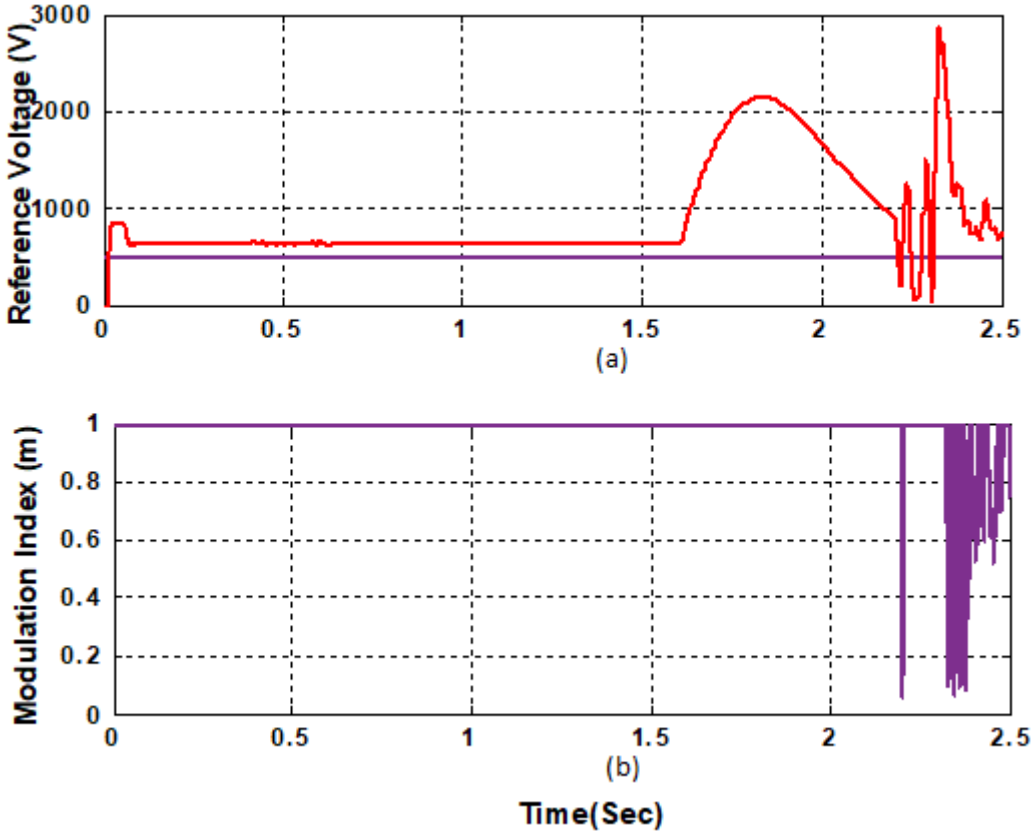

Figure 23. Performance of Vref–Vmean & Modulation Index with PSO-LSTM under dusty surface condition.

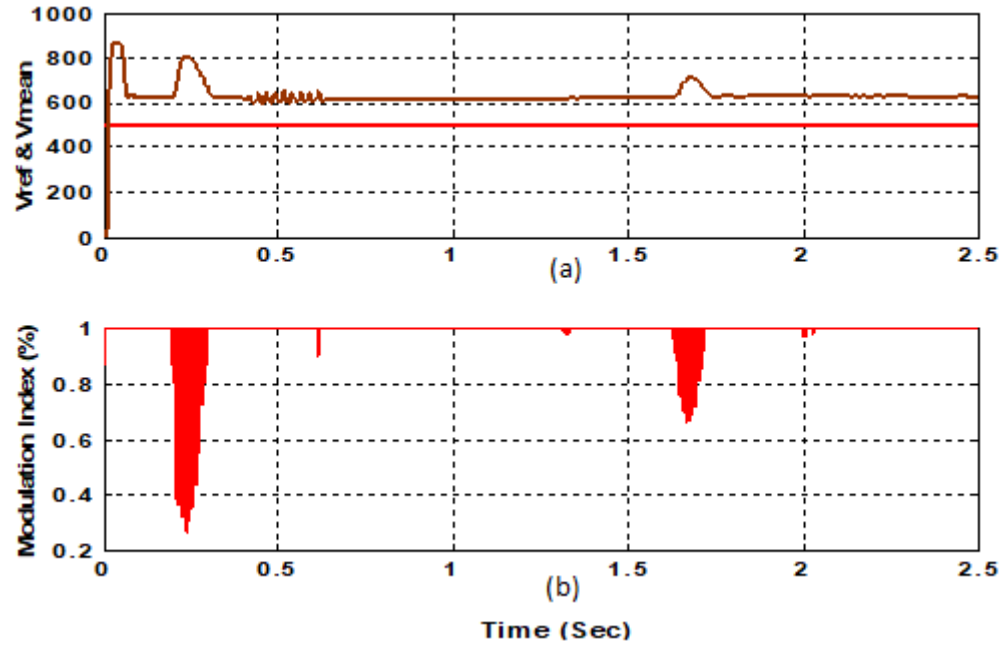

Figure 24. Performance of Vref–Vmean & Modulation Index with PSO-LSTM under greenhouse gas condition.

5. Conclusions

In the present research paper, a detailed investigation for maximum power point tracking using the P&O algorithm has been carried out. The genetic algorithm-based

benchmarking model shows that, during an increase in solar insolation, the oscillation around MPP shifts towards the right-hand side of the PV curve. This also reveals that instead of applying P&O to optimize at MPP, a predefined search space can be provided to the algorithm on the right-hand side of the PV curve around the MPP to decrease the oscillation. Again, based on the remarks provided by the genetic algorithm, the PSO-LSTM model has been developed and applied to MPPT with a P&O model with pre-defined right-hand side search space for reducing unwanted oscillation around the MPP. A detailed comparative analysis of three different case studies has also been investigated. According to the partial shading condition test, it is observed that with the proposed PSO-LSTM model, a standard deviation of 34.49 with a tracking time of 39.63 has been observed for 50% of the shading effect. Similarly, a tracking efficiency of 83.27% has been observed for partial shading conditions against 93.47% for normal efficiency. This also has been observed that the proposed algorithm is also 11.23% efficient as compared to the benchmarking model. Similarly, for the case-2 dusty surface, it is found that the tracking time is 4.93 ms for L-type dust and 8.67 ms for M-type dust.

Future research directions can be explored to enhance the use of LSTM for MPPT in photovoltaic (PV) systems. One direction could focus on evaluating the performance of LSTM-based MPPT under complex and dynamic shading conditions. Another area of research could involve optimizing the LSTM model architecture and hyperparameters to improve its accuracy and efficiency. Moreover, ensembling techniques, such as integrating LSTM with other machine learning models, could be studied to improve the accuracy of MPPT under varying operating conditions. Finally, assessing the implementation and effectiveness of LSTM MPPT in real-world PV systems could provide valuable insights into its practicality.

Author Contributions: Conceptualization, R.J., R.D. and K.J.R.; Investigation, S.C.S.; Methodology, R.J. and R.D.; Resources, P.K.P. and S.C.S.; Software, C.D.; Supervision, S.M.M.; Validation, R.D. and K.J.R.; Visualization, R.D. and K.J.R.; Writing—original draft, R.J.; Writing—review & editing, C.D. and S.M.M. All authors have read and agreed to the published version of the manuscript.

Funding: This research received no external funding.

Institutional Review Board Statement: Not applicable.

Informed Consent Statement: Not applicable.

Data Availability Statement: Not applicable.

Conflicts of Interest: The authors declare no conflict of interest.

References

1. Priya, T.H.; Parimi, A.M.; Rao, U.M. Development of hybrid controller for photovoltaic based DC-DC boost converter in DC grid connected applications. In Proceedings of the 2016 International Conference on Circuit, Power and Computing Technologies (ICCPCT), Nagercoil, India, 18–19 March 2016; pp. 1–6.
2. Hou, W.; Jin, Y.; Zhu, C.; Li, G. A novel maximum power point tracking algorithm based on glow worm swarm optimization for photovoltaic systems. *Int. J. Photoenergy* **2016**, *2016*, 4910862. [CrossRef]
3. Pilawa-Podgurski, R.C.N.; Perreault, D.J. Submodule integrated distributed maximum power point tracking for solar photovoltaic applications. *IEEE Trans. Power. Electron.* **2013**, *28*, 2957–2967 [CrossRef]
4. Kheldoun, A.B.R.B.; Bradai, R.; Boukenoui, R.; Mellit, A. Anewgolden section method based maximum power point tracking algorithm for photovoltaic systems. *Energy Convers Manag.* **2016**, *111*, 125–136. [CrossRef]
5. Sundareswaran, K.; Peddapati, S.; Palani, S. Application of random search method for maximum power point tracking in partially shaded photovoltaic systems. *IET Renew Power Gener.* **2014**, *14*, 670–678. [CrossRef]
6. Amir, A.; Selvaraj, J.; Rahim, N. Study of the MPP tracking algorithms: Focusing the numerical method techniques. *Renew. Sustain. Energy Rev.* **2016**, *62*, 350–371. [CrossRef]
7. Dash, R.; Paikray, P.; Swain, S.C. Active power filter for harmonic mitigation in a distributed power generation system. In Proceedings of the 2017 Innovations in Power and Advanced Computing Technologies (i-PACT), Vellore, India, 21–22 April 2017; pp. 1–6. [CrossRef]
8. Tajuddin, M.F.N.; Arif, M.S.; Ayob, S.M.; Salam, Z. Perturbative methods for maximum power point tracking (MPPT) of photovoltaic (PV) systems: A review. *Int. J. Energy Res.* **2015**, *39*, 1153–1178. [CrossRef]

9. Chapman, P.; Esram, T. Comparison of photovoltaic array maximum power point tracking techniques. *IEEE Trans Energy Convers.* **2007**, *22*, 439–449.
10. Patnaik, B.; Swain, S.C.; Dash, R.K. An Experimental Analysis of Solar PV on Higher Concentration of Methane. In Proceedings of the 2022 IEEE India Council International Subsections Conference (INDISCON), Bhubaneswar, India, 15–17 July 2022; pp. 1–5. [CrossRef]
11. Sera, D.; Kerekes, T.; Teodorescu, R.; Blaabjerg, F. Improved MPPT algorithms for rapidly changing environmental conditions. In Proceedings of the 2006 12th International Power Electronics and Motion Control Conference, Portoroz, Slovenia, 30 August–1 September 2006; pp. 1614–1619.
12. Narsingoju, K.; Busa, V.; Kumar, G.V. Simulation analysis of maximum power control of photovoltaic power system. *Int. J. Adv. Electr. Electron Eng.* **2012**, *1*, 9–14.
13. Patnaik, B.; Swain, S.C.; Dash, R. A Study on Effect of GHG on the Performance of Grid Connected Solar PV System. In Proceedings of the 2022 IEEE India Council International Subsections Conference (INDISCON), Bhubaneswar, India, 15–17 July 2022; pp. 1–4. [CrossRef]
14. Sakib, N.; Kabir, M.W.U.; Subbir, M.; Alam, S. A comparative study of flower pollination algorithm and bat algorithm on continuous optimization problems. *Int. J. Appl. Inf. Syst.* **2014**, *7*, 13–19. [CrossRef]
15. Yang, B.; Zhong, L.; Zhang, X.; Shu, H.; Yu, T.; Li, H.; Jiang, L.; Sun, L. Novel bio-inspired memetic salp swarm algorithm and application to MPPT for PV systems considering partial shading condition. *J Clean Prod.* **2019**, *215*, 1203–1222. [CrossRef]
16. Kumar, C.; Rao, R. A novel global MPP tracking of a photovoltaic system based on whale optimization algorithm. *Int. J. Renew. Energy Dev.* **2016**, *5*, 225–232. [CrossRef]
17. Mohanty, S.; Subudhi, B.; Ray, P.K. A new MPPT design using grey wolf optimization technique for photovoltaic system under partial shading conditions. *IEEE Trans. Sustain. Energy* **2016**, *7*, 181–188. [CrossRef]
18. Mansoor, M.; Feroz Mirza, A.; Ling, Q. Harris hawk optimization-based MPPT control for PV systems under partial shading conditions. *J. Clean Prod.* **2020**, *274*, 122857. [CrossRef]
19. El-Helw, H.M.; Magdy, A.; Marei, M.I. A hybrid maximum power point tracking technique for partially shaded photovoltaic arrays. *IEEE Access* **2017**, *5*, 11900–11908. [CrossRef]
20. Paul, R.; Dash, R.; Swain, S.C. Design & Analysis of Current Controller for SPV Grid Connected System through Hysteresis CCT. In Proceedings of the 2018 International Conference on Applied Electromagnetics, Signal Processing and Communication (AESPC), Bhubaneswar, India, 22–24 October 2018; pp. 1–6. [CrossRef]
21. Liu, C.-H.; Gu, J.-C.; Yang, M.-T. A Simplified LSTM Neural Networks for One Day-Ahead Solar Power Forecasting. *IEEE Access* **2021**, *9*, 17174–17195. [CrossRef]
22. Kong, W.C.; Dong, Z.Y.; Jia, Y.W.; Hill, D.J.; Xu, Y.; Zhang, Y. Short-Term Residential Load Forecasting Based on LSTM Recurrent Neural Network. *IEEE Trans. Smart Grid* **2019**, *10*, 841–851. [CrossRef]
23. Premkumar, M.; Sowmya, R. Certain study on MPPT algorithms to track the global MPP under partial shading on solar PVmod-431 ule/array. *Int. J. Comput. Digit. Syst.* **2019**, *8*, 405–416. [CrossRef]
24. Ali, S.; Bhargava, A.; Saxena, A.; Kumar, P. A Hybrid Marine Predator Sine Cosine Algorithm for Parameter Selection of Hybrid Active Power Filter. *Mathematics* **2023**, *11*, 598. [CrossRef]
25. Aziz, R.M.; Mahto, R.; Goel, K.; Das, A.; Kumar, P.; Saxena, A. Modified Genetic Algorithm with Deep Learning for Fraud Transactions of Ethereum Smart Contract. *Appl. Sci.* **2023**, *13*, 697. [CrossRef]
26. Sahoo, S.; Swain, S.C.; Dash, R. A Novel Flower Pollination Method for Unit Price Estimation in a Microgrid. In Proceedings of the 2022 3rd International Conference for Emerging Technology (INCET), Belgaum, India, 27–29 May 2022; pp. 1–5. [CrossRef]
27. Abd-Elazim, S.M.; Ali, E.S. Imperialist competitive algorithm for optimal STATCOM design in a multimachine power system. *Int. J. Electr. Power Energy Syst.* **2016**, *76*, 136–146. [CrossRef]
28. Patnaik, B.; Swain, S.C.; Rout, U.K.; Dash, R. Performance of Solar PV under higher Concentration of Carbon dioxide and Methane. In Proceedings of the 2022 Trends in Electrical, Electronics, Computer Engineering Conference (TEECCON), Bengaluru, India, 26–27 May 2022; pp. 113–118. [CrossRef]
29. Ballaji, A.; Dash, R.; Subburaj, V.; Kalvakurthi, J.R.; Swain, D.; Swain, S.C. Design & Development of MPPT Using PSO With Predefined Search Space Based on Fuzzy Fokker Planck Solution. *IEEE Access* **2022**, *10*, 80764–80783. [CrossRef]
30. Patnaik, B.; Swain, S.C.; Rout, U.K.; Dash, R. An Experimental Investigation of Co2 Concentration on Solar PV Performance using SVM. In Proceedings of the 2021 Innovations in Power and Advanced Computing Technologies (i-PACT), Kuala Lumpur, Malaysia, 27–29 November 2021; pp. 1–6. [CrossRef]
31. Ramadan, A.; Kamel, S.; Hassan, M.H.; V´eliz, T.M.; Eltamaly, A.M. Parameter Estimation of Static/Dynamic Photovoltaic Models Using a Developed Version of Eagle Strategy Gradient-Based Optimizer. *Sustainability* **2021**, *13*, 13053. [CrossRef]
32. Dash, R.; Behera, P.R.; Ali, S.M. Hybrid system for meeting global energy demand with solar PV and wind system. In Proceedings of the 2014 International Conference on Control, Instrumentation, Communication and Computational Technologies (ICCICCT), Kanyakumari, India, 10–11 July 2014; pp. 388–392. [CrossRef]
33. Dash, R.; Swain, S.C. Effective Power quality improvement using Dynamic Activate compensation system with Renewable grid interfaced sources. *Ain Shams Eng. J.* **2018**, *9*, 2897–2905. [CrossRef]
34. Abdul-Kalaam, R.; Muyeen, S.; Al-Durra, A. Review of maximum power point tracking techniques for photovoltaic system. *Glob. J. Control Eng. Technol.* **2016**, *2*, 8–18.

35. Swain, S.C.; Dash, R.; Ali, S.M.; Mohanta, A.K. Performance evaluation of photovoltaic system based on solar cell modelling. In Proceedings of the 2015 International Conference on Circuits, Power and Computing Technologies [ICCPCT-2015], Nagercoil, India, 19–20 March 2015; pp. 1–6. [CrossRef]
36. Premkumar, M.; Sumithira, T.R. Humpback whale assisted hybrid maximum power point tracking algorithm for partially shaded 445 solar photovoltaic systems. *J. Power Electron.* **2018**, *18*, 1498–1511.